Dalton Transactions

ROYAL SOCIETY OF CHEMISTRY

PAPER

View Article Online
View Journal | View Issue

Cite this: *Dalton Trans.*, 2024, **53**, 6709

Cu(dppf) complexes can be synthesized from Cu-exchanged solids and enable a quantification of the Cu-accessibility by ^{31}P MAS NMR spectroscopy†

Elif Kaya, Daniel Dittmann, Maximilian Schmidt and Michael Dyballa *

Received 17th January 2024,
Accepted 21st March 2024

DOI: 10.1039/d4dt00147h

rsc.li/dalton

Herein, we apply three different copper-exchanged materials (Na–[Al]SBA-15, silica, Na–MCM-22) as hosts for a direct synthesis of Cu^{I}(1,1′-bis(diphenylphosphino)ferrocene = dppf) complexes in cationic ion exchange position. Using ^{31}P MAS NMR spectroscopy, we show that identical complexes as after ion exchange are generated if the solids are applied as reactants directly. The homogeneity of copper exchanges is evaluated by EDX spectroscopy. Both Cu^{I} and Cu^{II} result in the formation of complexes, thereby oxidizing dppf. Cu-particles were not reactive. Optimized conditions for a maximized complex formation are identified applying quantitative ^{31}P MAS NMR spectroscopy and ICP-OES. Only accessible copper in cationic position of the solids forms the complexes. This enables a quantification of the amount of copper in mesopores *vs.* the total copper amount. Thus, besides a new synthesis of the complex a suitable method for quantitative elucidation of the location of copper cations is demonstrated herein.

Introduction

Most industrially relevant large-scale conversions are conducted catalytically. Usually, catalyst and reactant and/or products are thereby present in different phases. The support in such heterogeneous catalysis systems is usually a solid, as this can cost-efficiently be separated from the reaction mixture.[1] Typical solid catalysts are porous in order to enlarge the surface area for an efficient contact between reaction medium and catalyst. Exemplary supports are zeolites, metal–organic frameworks, and mesoporous materials.[2–5] The diameter of the pores determines the dimension of the species that can be hosted, which leads to shape-selectivity effects during catalysis.[6] The support must furthermore stabilize the catalytically active sites in the solid. Copper is a frequently investigated active site, and a variety of ways is applied to support active copper in form of a heterogeneous catalyst.

One form of stabilization is ion exchange into the cation position of bridging Si(OX)Al groups (with X = monovalent cation) that are found in silicoaluminates.[2,7] For catalyst synthesis, the Cu^{II} ions are typically ion exchanged into porous silicoaluminates prior to the conversion of the hydrocarbons. This metal cations catalyse, for example, the selective oxidation of methane and ethane by solid catalysts.[8–14] In contrast to heterogeneous catalysis, where ion exchange is applied frequently, this is a seldom investigated technique for metalorganic complex immobilization. Copper complexes can be (1) adsorbed onto the surface, (2) bound to the surface using it as ligand (referred to as surface organometallic chemistry, SOMC), (3) bound to the surface using a linker (molecular heterogeneous catalysts) and finally (4) charged complexes can be immobilized by ion exchange.[15–18] In the case of surface organometallic chemistry (SOMC), the complex formation takes place inside the pores with the surface as a ligand.[15,16,19] A potential application of SOMC is also the formation of defined nanoparticles[20] or the better understanding of processes occurring on often ill-defined heterogeneous catalysts.[21,22] Counter-intuitively also for covalently bound molecular heterogeneous catalysts a strong interaction with the surface can be present.[15,16] Such strong surface interactions impact on the catalytic performance of the materials. Complexes formed by methods of SOMC and likewise molecular heterogeneous catalysts form part of the surface or are covalently bound to the surface, respectively, and used for catalytic applications. As synthesis of complexes on a solid support means also removing these complexes in a second step, thus, only ion exchange and adsorption remain as industrially feasible pathways. Herein we synthesize complexes in ion exchange position of a solid support to enable their later release.

In catalytic reactions, interactions between copper and surface play an important role. For example, copper-based cat-

Institute of Technical Chemistry, University of Stuttgart, Pfaffenwaldring 55, 70569 Stuttgart, Germany. E-mail: michael.dyballa@itc.uni-stuttgart.de

† Electronic supplementary information (ESI) available. See DOI: https://doi.org/10.1039/d4dt00147h

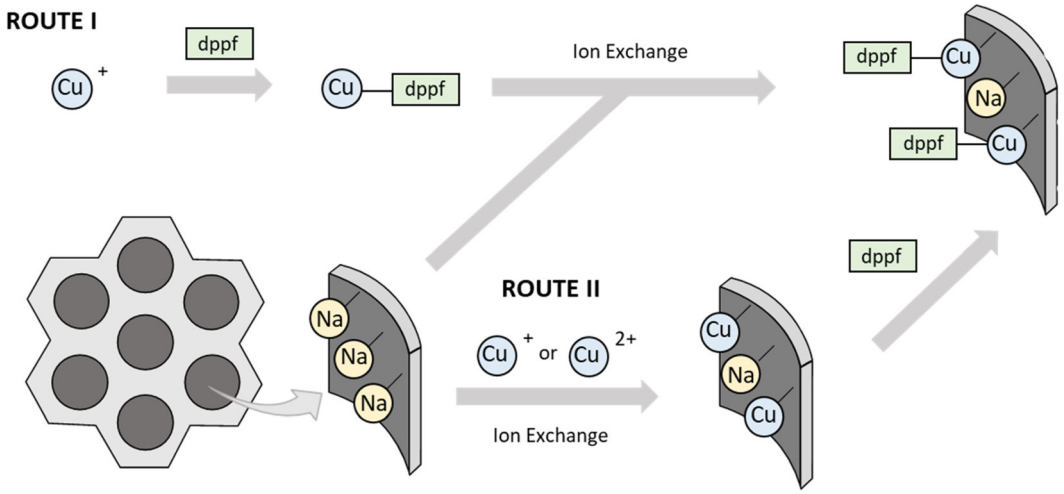

Scheme 1 Reaction scheme for visualizing the synthesis of Cu^{I}(dppf) complexes in counter ion position synthesized by ion exchange (route I) or by reaction with $Cu^{I/II}$ counter ions (route II).

alysts immobilized on Al_2O_3 were shown to outperform their homogeneous counterparts in terms of selectivity in atom-transfer radical cyclizations.[23] Also location-dependent selectivity changes during catalysis by Rh-complexes in 1,2-additions were found, indicating that the location of the active site within the solid is important for the application as catalyst.[24] Unfortunately, if immobilized in porous materials, such complexes remain often in the outer parts of the catalysts.[24,25] The reason is the large diameter of the complexes and the strong interactions with the surface. Conclusively, it was also shown that ion exchange can lead to a very strong binding between Cu^{I}(dppf) (dppf = 1,1′-bis(diphenylphosphino)ferrocene) complexes and surfaces.[26] This motif was previously identified to be interesting for electrochemical or anticancer applications.[27,28] In this favourable cases, metalorganic complexes bear a phosphorus nucleus ($I = \frac{1}{2}$) which can be investigated quantitatively using ^{31}P MAS NMR spectroscopy.[29–34] Finally it can be summarized that techniques to finely distribute such complexes in pores are of interest for the community. We herein thus also focus on how synthesized cationic complexes as counter ions in ion exchange position can be applied to characterize the support.

The typical way to place a cationic complex in counter ion position of an inorganic support is as follows: first the metalorganic complex, in this case consisting of Cu^{I} and dppf, is synthesized. Then the cationic complex is ion-exchanged into the solid. This procedure is visualized in route I in Scheme 1.[26] In this work, it shall thus be investigated weather a direct Cu^{I}(dppf) complex formation in an ion exchanger is possible. This new, alternative route involves a direct synthesis of the copper-exchanged solid and then the dppf is reacted directly with the cations. A schematic presentation of this procedure is shown in route II in Scheme 1. To maximize the surface and the amount of ion exchange sites, the copper-exchanged aluminated [Al]SBA-15 is used as support. This amorphous silicoaluminate has a large surface area and is capable of a quantitative ion exchange inside its mesopores of usually 6 nm and above, which is large enough to host metalorganic complexes inside the pores.[35] Typical heterogeneous catalysts contain copper in its highest oxidation state (Cu^{II}). It should be noted that this cation might form a variety of oxidizing copper-oxo species, for example Cu^{II}(OH), depending on the surface of the support and the conditions.[36–40] Thus it shall be tested if the complex formation occurs also with a precursor containing this cation. In route II the complex forms inside a porous solid. It is important to note that a complex formation is only possible if (1) the dppf has access to the copper and if (2) there is enough space available to form a complex.[32] A similar picture is observed if noble metals react with phosphines in inorganic complexes as triphenylphosphines and higher analogues. Also in this case a complex forms directly inside a mesopore that is large enough to host the resulting complex.[41,42] The sensitivity of synthesis route II for space and accessibility determined by the solid can be used as tool for characterization. In other words, the direct complex synthesis enables information about the location of the formerly present ions inside the solid. This makes route II interesting for quantitative elucidating the spatial distribution of ion exchanged copper.

Results and discussion

Physicochemical characterization of supports

In this work three different supports for copper are applied. The standard characterization of these materials is found in Table 1. For checking the presence of regular mesoporosity, small-angle X-ray powder diffraction patterns (XRD) were recorded (see Fig. S1 in the ESI†). Likewise, the crystalline zeolite Cu–MCM-22 was investigated by wide-angle XRD (see Fig. S2 in the ESI†). Both patterns agree with those reported in literature for SBA-15 and MCM-22.[35,43,44] Thus, we conclude

Table 1 Physicochemical characterization data of the materials under study

Material	Si/Al[a]	Cu[a] [mmol g^{-1}]	BET surface[b] [m^2 g^{-1}]	V_{pore}[b] [ml g^{-1}]	V_{micro}[b] [ml g^{-1}]	V_{meso}[b] [ml g^{-1}]	Si(OH) density[c] [mmol g^{-1}]	BAS content H-form[d] [mmol g^{-1}]
Cu–[Al]SBA-15	14	0.27	850	1.34	—	1.34	1.19	—
Cu@silica (A200)	>1700	1.26	185	0.24	—	0.24	0.39	—
Cu–MCM-22	19	1.02	630	0.79	0.18	0.61	0.18	0.17

[a] Determined by ICP-OES, error ±1. [b] From N_2 physisorption. [c] From ^{1}H MAS NMR after subtracting BAS density. [d] From ^{1}H MAS NMR after NH_3 adsorption.

that our materials have an intact meso- or micropore structure. The Cu–[Al]SBA-15 synthesized with a Si/Al ratio of 14 shows in comparison to literature a higher BET surface area.[35] This is a result of the large surface area of the siliceous parent SBA-15 (1160 m^2 g^{-1}) before alumination. In accordance with literature,[35] no micropores were detected after alumination while a large mesopore volume V_{meso} of 1.34 ml g^{-1} was maintained. Thus, the support can not only host cations but also larger complexes within its mesopores. The silica A200 is a commercial, fumed silica support with negligible aluminum impurities, a BET surface area of 185 m^2 g^{-1}, and secondary mesopores as described previously.[45] The state of aluminum in Cu–[Al]SBA-15 and Cu–MCM-22 was investigated by ^{27}Al MAS NMR spectroscopy (see Fig. S3 in the ESI†). The spectrum of Na–[Al]SBA-15 contains a single peak at a chemical shift of δ_{27Al} = 53 ppm. This peak is assigned to a tetrahedral aluminum within the framework and proves a maximum in well-exchangeable cationic sites.[35] In silica A200, we find no aluminum, neither by ICP-OES nor by ^{27}Al MAS NMR. The ^{27}Al MAS NMR spectrum of MCM-22 shows two peaks. A peak at δ_{27Al} = 56 ppm can again be assigned to aluminum in the framework. The peak at δ_{27Al} = 0 ppm indicates presence of extra-framework aluminum, which agrees well with previous findings on the aluminum state in this zeolite structure.[44]

The copper content of the materials was investigated by ICP-OES (see Table 1). Cu–[Al]SBA-15 has thus 0.27 mmol g^{-1} copper cations. In addition to the directly evaluation of copper, we also cross-checked by ICP-OES that the Na-content of the material decreased after ion exchange, from 1.07 to 0.34 mmol g^{-1} Na^+. The larger decrease in mmol g^{-1} is reasonable, as the 2-fold charged copper cations will exchange cations stoichiometrically. Furthermore, an incomplete ion exchange indicates that some Na-cations could not be exchanged. For a better understanding, despite Na-cations are still present, the resulting material is labeled Cu–[Al]SBA-15. The copper content of impregnated silica A200 (labeled Cu@silica) was 1.26 mmol g^{-1} while the copper content of the ion-exchanged zeolite Cu–MCM-22 was 1.02 mmol g^{-1}. SEM images of the support after ion exchange with copper are provided in Fig. 1. The elongated structures of SBA-15 particles are typical for this mesoporous material.[35] To prove a homogeneous alumination of the SBA-15 material and a homogeneous exchange with copper, EDX mappings were performed. The Si–EDX mapping resembles the structures of the SEM as this element constitutes the backbone of the material.

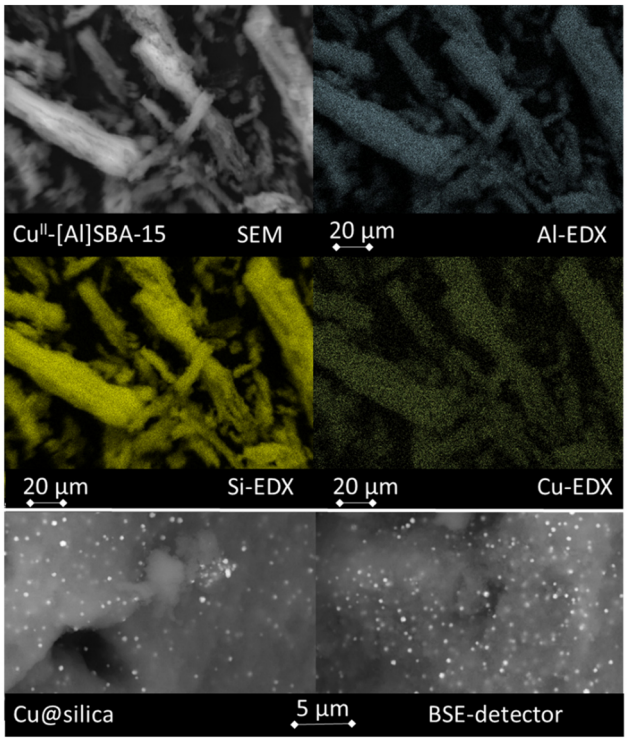

Fig. 1 SEM and EDX screenings on copper-exchanged [Al]SBA-15 (top). Characteristic Cu-particles formed on Cu@silica are revealed by the BSE-detector.

The Al–EDX mapping shows identical structures, in lower intensity due to the lower abundance of aluminum. Absence of bright spots indicates absence of aluminum deposits and conclusively, a homogeneous alumination distribution was achieved by alumination, as expected from tests in previous work.[35] Also the Cu–EDX mapping resembles the structures from the SEM pictures. Again, an absence of bright spots indicates a homogeneous distribution of ion exchanged copper and absence of copper particles. As further proof of a homogeneous copper distribution, the backscattered electron detector (BSE-detector) was applied. No bright spots appeared and thus no copper particles formed. We conclude that the copper cations are homogeneously stabilized at ion exchange sites associated with aluminum and that no copper deposits were formed on Cu–[Al]SBA-15. Comparable figures of EDX on Cu@silica and Cu–MCM-22 are found in Fig. S4 and S5 in the

ESI.† Thereby, for Cu–MCM-22 a similar picture as for Cu–[Al]SBA-15 is observed as also here all copper is introduced by ion exchange. In contrast, bright spots occur on Cu@silica when using the BSE-detector. Thus, Cu-particles form on the silica surface as result of the impregnation and the absence of stabilizing ion exchange sites. These Cu-particles give characteristic bright spots in the BSE-detector and indicate a bad stabilization of cationic copper.[46]

The density of Si(OH) groups on the material surfaces was quantified applying ^{1}H MAS NMR spectroscopy. A density of 1.19 mmol g^{-1} was found for Na–[Al]SBA-15 and agrees well with the 1.14 mmol g^{-1} reported previously.[45] Thus, this surface can be considered polar, compared to the other two material surfaces. A lower Si(OH) density of 0.24 mmol g^{-1} was found for silica A200, in agreement with a literature value of 0.39 mmol g^{-1}.[45] The Si(OH) density of the zeolite H–MCM-22 is, with 0.18 mmol g^{-1}, comparable. The higher Si(OH) density on [Al]SBA-15 results from the amorphous surface structure. In contrast, on the crystalline structure of MCM-22 or on the heat-treated fumed silica surface more Si(OH) groups formed siloxane bridges upon water release. MCM-22 and [Al]SBA-15 are aluminum-doted, which results in Brønsted acid site (BAS) formation on the material H-form (after ion exchange).[7] Quantitative ^{1}H MAS NMR spectroscopy was thus applied to evaluate the acidity of the respective H-forms (see Fig. S6 in the ESI†). All materials show peaks of Si(OH) groups at a chemical shift of δ_{1H} = 1.8 ppm., while broad peaks at ~2.5 ppm are assigned to interacting Si(OH) groups. The latter peak broadens for Na–[Al]SBA-15 after NH_3-loading as a result of the heat treatment applied during NH_3-desorption.[35] The H–MCM-22 shows peaks at 3.9 ppm and above, caused by Brønsted acidic bridging Si(OH)Al groups in free or disturbed state.[47–49] These groups react with NH_3 to form NH_4^+ which gives a quantifiable peak at 6.4 ppm.[32,50] The peak intensity indicates the accessibility of 0.17 mmol g^{-1} BAS. This is low compared to the ~0.8 mmol g^{-1} BAS expected from the Si/Al ratio. However, this is reasonable due to the formation of EFAl, as it was indicated by ^{27}Al MAS NMR spectra (*vide supra*). This is in-line with previous findings for similar H–MCM-22.[44] Note that MCM-22 was copper ion exchanged from its Na-form and that all copper-bearing materials applied in this study for complex formation experiments were free of detectable BAS.

Reaction of Cu–[Al]SBA-15 with dppf

The formed Cu^{I}(dppf) complexes are in the following investigated using ^{31}P MAS NMR spectroscopy (see Fig. 2). The neat dppf results in a slim signal at a chemical shift of δ_{31P} = −15 ppm. From literature it is known that adsorption of phosphines at silicoalumina surfaces usually leads to downfield shifts of the peaks.[24,41] In seldom cases also for dppf, an additional peak at −9 ppm, caused by dppf in surface interaction, is found herein. In Fig. 1, below the spectrum of neat dppf, the benchmark in form of an ion exchanged complex Cu–[Al]SBA-15, synthesized according to route I in Scheme 1, is shown. The spectrum contains a multitude of lines, since each resonance is split into $2I + 1 = 4$ individual lines due to ^{1}J coupling of the ^{31}P nuclei of the dppf ligand with the ^{63}Cu/^{65}Cu (I = 3/2) cations. We see that there are two different spins associated with the central copper and, due to a higher natural abundance of ^{63}Cu, the lines belonging to ^{65}Cu are less intense. Due to a $\gamma(^{65}Cu)/\gamma(^{63}Cu)$ = 1.07 larger ^{1}J coupling, the lines belonging to ^{65}Cu complexes are furthermore found outside of the lines belonging to ^{63}Cu complexes.[51] As preciously shown, both ^{31}P nuclei present in the dppf become inequivalent upon ion exchange.[26] Thus, a characteristic splitting into 8 overlapping lines is observed (4 lines for each ^{31}P nucleus in dppf). The outer lines of the coupling pattern are found at chemical shifts of about δ_{31P} = −7 and −37 ppm, respectively. This supports the conclusion, that the herein investigated complexes are cations in ion exchange position and agrees with literature findings, ^{1}H–^{31}P FSLG HETCOR spectra provided herein (*vide infra*), and the spectra of similar ion exchanged materials provided previously.[26] Next, the reaction of Cu^{I}–[Al]SBA-15 with dppf was investigated. For the reaction, a 1 : 1 stoichiometry between Cu^{I} and dppf was applied. An identical spectrum as for the benchmark is received and it will later become important to remark that no additional peaks are found at higher or lower field, respectively. This clarifies, that exclusively Cu^{I}(dppf) complexes, but no by-pro-

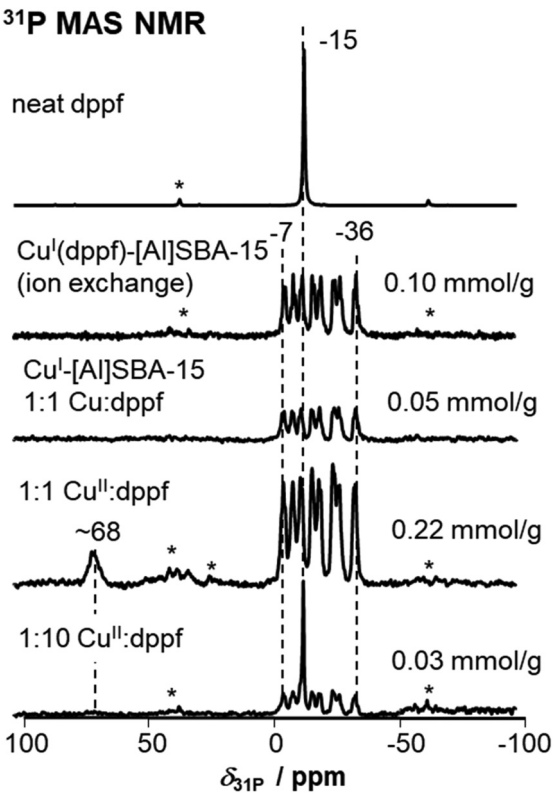

Fig. 2 ^{31}P MAS NMR spectra of (from top to bottom) neat dppf, Cu^{I}(dppf) ion exchanged into Na–[Al]SBA-15, dppf reacted with Cu^{I}–[Al]SBA-15, and dppf reacted with Cu^{II}–[Al]SBA-15. The stoichiometry 1 : 1 and 1 : 10 indicates the molar rations between copper and dppf, while the loading amounts in mmol g^{-1} indicate the amount of Cu^{I}(dppf) derived from quantitative ^{31}P MAS NMR spectroscopy.

ducts were formed upon reaction of Cu^{I} in cationic ion exchange position with dppf. The complexes can be quantified with an external standard applying ^{31}P MAS NMR spectroscopy. This results in amounts of 0.10 to 0.05 mmol g^{-1} complexes within the mesoporous [Al]SBA-15 support after ion exchange of reaction with Cu^{I}, respectively (see also quantitative indications in Fig. 2).

In a next step, the reaction of dppf with Cu^{II} is addressed. This formation of Cu^{I}(dppf) requires a reduction of the Cu^{II} cations present. The species responsible for oxygen-transfer could be a $Cu(OH)^{+}$ unit that forms upon ion exchange in aqueous media to balance the charge of Cu^{II} on an ion exchange site with single negative charge. Furthermore, similar sites were identified by XAS in copper-exchanged zeolite catalysts.[39,52] Additional peaks at higher chemical shift at δ_{31P} of ~68 ppm appear. Typically, peaks at such low-field chemical shift of $\delta_{31P} \approx 68$ ppm originate from the oxidation of phosphines to the corresponding phosphine oxide, which is supported by previous work on a variety of phosphines.[24,53–56] Unfortunately, it was herein not possible to isolate this oxidation product and to further characterize it. As this happens only in case of Cu^{II} presence, oxidation due to oxygen impurities during sample handling can be excluded. Also a previous calcination at 823 K after copper ion exchange of Cu–[Al]SBA-15 leads to identical ^{31}P MAS NMR spectra. This excludes that any surface impurity caused this peak. It is thus associated with dppf oxidation to the corresponding oxide. The ^{31}P MAS NMR spectrum of the resulting Cu^{I}(dppf) is identical to the spectra recorded after ion exchange or reaction with Cu^{I} (*vide supra*). In accordance with the reactivity of other phosphines we conclude that herein the dppf reduces the Cu^{II} to Cu^{I}. The latter subsequently forms a complex identical to those received after ion exchange of Cu^{I}(dppf) into the material or after reaction with Cu^{I}–[Al]SBA-15. Quantification shows that a reaction in a 1 : 1 stoichiometry between Cu^{II} and dppf leads to an amount of 0.22 mmol g^{-1} Cu^{I}(dppf) complex formed. This is a reasonable quantity with respect to the 0.27 mmol g^{-1} copper initially present on the Cu–[Al]SBA-15 material. Note that not all copper has reacted to form complexes. Furthermore, the reaction with dppf was also tested in absence of solvent to check if solvent is necessary. This was done according to the solid state loading approach previously applied for loading a variety of other phosphines and phosphine oxides on solids.[35,42,57–59] Briefly, the Cu–[Al]SBA-15 solid was mixed with neat, solid dppf and the mixture was heated over 2 h with a heating rate of 1 K min^{-1} at 333 K under N_2. However, on Cu–[Al]SBA-15 no Cu^{I}(dppf) complex formed and only the slim ^{31}P MAS NMR peak associated with the neat dppf was found. We conclude that the formation of Cu^{I}(dppf) complexes from cationic copper requires a solvent. It is not relevant if the solvent is acetonitrile or ethanol, however, a larger quantity of the complex forms if ethanol is applied.

^{1}H–^{31}P FSLG HETCOR was performed to further clarify the identity of complexes synthesized by the two routes indicated in Scheme 1. For the 2D spectra in Fig. 3 it is immediately noted that similar correlations exist for both synthesis routes I and II. Correlation peaks at $\delta_{1H} \approx 4$, 5 and 7 ppm are associated with the protons of the cyclopentadienyl and phenyl rings, respectively. The splitting of the cyclopentadienyl ring protons into two individual signals with 4 lines each is caused by magnetic inequivalence of the ^{31}P nuclei of dppf upon ion exchange (*vide supra* and elsewhere[26]). As result, $^{1}J(^{63/65}Cu, ^{31}P)$ scalar couplings of 1200 and 1340 Hz are found, in agreement with previous findings.[26] A proton at $\delta_{1H} \approx 10$ ppm is found in both 2D spectra and indicates an interaction between complexes and Si(OH) on the surface. Thus, it was verified that identical structures have formed within mesoporous [Al]SBA-15 also after reaction of the copper-exchanged Cu–[Al]SBA-15 with dppf. This is the first proof that both route I and route II indicated in Scheme 1 are applicable to generate cationic Cu^{I}(dppf) complexes.

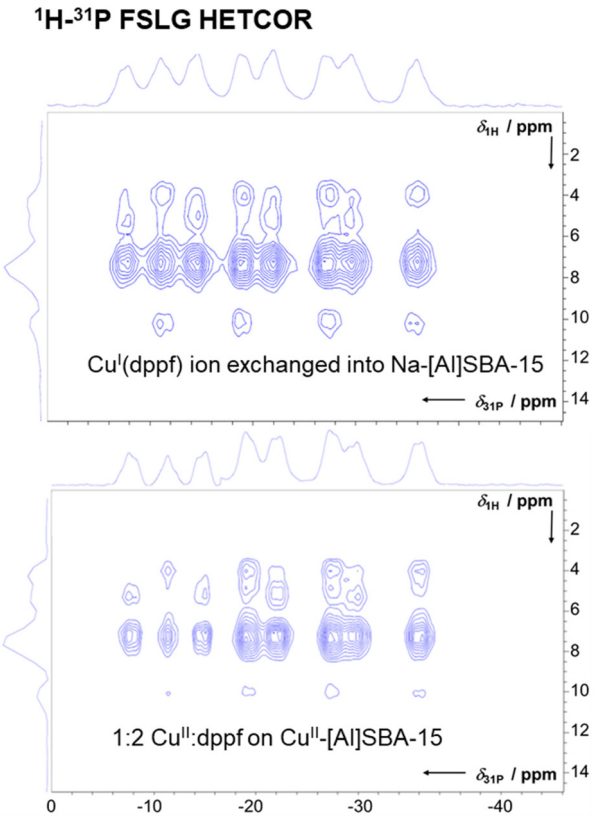

Fig. 3 ^{1}H–^{31}P FSLG HETCOR spectra on (top) Na–[Al]SBA-15 after ion exchange of Cu^{I}(dppf) complexes and (bottom) after reaction of dppf with Cu^{II}–[Al]SBA-15 with indicated loading stoichiometry 1 : 2 Cu : dppf.

Quantitative study of the complex formation

Quantitative ^{31}P MAS NMR spectroscopy applied on (neat) metalorganic complexes is hampered by usually long T_1-times.[29–31,33,34,51,60] However, if the phosphine is tightly bound to the surface the T_1-relaxation of the ^{31}P nuclei is significantly decreased.[33,42] In order to approximate the T_1-time we performed a delay time variation (see Fig. S7 and S8 in the ESI†). For the neat Cu^{I}(dppf) complex, an increasing ^{31}P signal intensity is found for increasing delay time between scans from 5 to

240 s. In other words, even 240 s delay yields no quantitative spectrum of the pure complex under our measurement conditions (see Fig. S7 in the ESI†). Also for neat dppf, the peak intensity at δ_{31P} = −15 ppm is not constant after 240 s delay time. However, the relaxation behavior changes dramatically if the complex is ion exchanged into the support. In our case, a delay between scans of 10 s or longer is sufficient, to yield spectra of similar intensity (see Fig. S8 in the ESI†). The shorter T_1-time is rationalized by the strong interaction between complex and surface (see cross-peak with Si(OH) δ_{1H} ≈ 10 ppm in Fig. 3) and the close proximity to ^{27}Al in the ion exchange position. Conclusively, delays above 10 s were quantitative. However, to include a safety threshold, herein 60 s delay were applied for quantitative evaluation of the ^{31}P spectra. We furthermore verified that for each individual sample that indeed quantitative spectra were gained. Therefore, a second measurement with a delay time of 40 s was performed. Only if peak intensities after applying 40 and 60 s delay were identical, a quantification was performed. It is fair to note that this was the case for all herein investigated complexes. To reveal potential pitfalls, it is worth showing ^{1}H MAS NMR spectra of materials (see Fig. S9 in the ESI†). Peaks of ethanol appear at δ_{1H} = 3.6 and 1.2 ppm and indicate its adsorption on the surface. The peak intensity, and thus the quantity of adsorbed ethanol, varies from sample to sample. However, for a quantification the dry material mass needs to be determined. This makes a treatment in vacuum, to remove adsorbed ethanol prior a mass determination, necessary. The successful ethanol removal can, in reverse, be checked by ^{1}H MAS NMR.

In Fig. 2 it was found that the stoichiometry between copper and dppf ligand impacts the amount of finally formed complexes. Because, counter-intuitively, fewer Cu^{I}(dppf) complexes (0.03 mmol g^{-1}) were formed after reaction in 1 : 10 Cu : dppf stoichiometry than in 1 : 1 stoichiometry (0.22 mmol g^{-1}). Furthermore, a strong and slim peak at δ_{31P} = −15 ppm is present after probing in 1 : 10 Cu : dppf stoichiometry. This peak belongs to neat dppf, which indicates that previously formed Cu^{I}(dppf) complex decomposed over time. To further investigate this decomposition, ^{31}P MAS NMR measurements on the sample (1 : 10 stoichiometry) were performed over a period of several days (see Fig. 4). Thereby, a decreasing intensity of the peaks associated with the Cu^{I}(dppf) complex and in parallel an increasing intensity of the peak of neat dppf at δ_{31P} = −15 ppm is observed. This supports a decomposition of the initially formed Cu^{I}(dppf) complexes within the time span of 43 h. Such a decomposition is only observed, if dppf is used in large excess. Conversely, in case of a 1 : 1 stoichiometry, samples are often stable over days without loss in signal intensity and thus complex decomposition. Of course, this requires storage in a closed, air-free container. The stability of the complex in this case proves that the dppf is stable against oxidation over time and supports that it is only oxidized in presence of Cu^{II} cations (*vide supra*).

Next, optimized formation conditions for a maximized Cu^{I}(dppf) complex formation were identified. First the stoichiometry between dppf and Cu^{II} ions during reaction was addressed (see Fig. 5a). A 1 : 1 stoichiometry between Cu^{II} and dppf results in the largest complex amount formed. Conversely, more dppf applied during reaction leads to a strong decrease of the number of complexes finally observed. Apart from complex decomposition, proven in Fig. 4, leaching of copper cations could potentially be a reason for a decreased complex amount. The copper-content of the samples after loading was thus cross-checked by ICP-OES (see Fig. 5(b)). After 2 h reaction time in a 1 : 1 stoichiometry the initial copper content is maintained (0.27 mmol g^{-1}). As, according to ^{31}P MAS NMR spectroscopy, 0.22 mmol g^{-1} complex was formed, it is calculated that 81% of the initially available copper reacted to Cu^{I}(dppf) complexes. This shows that the present copper cations reacted nearly quantitatively to the complex. The 19% discrepancy is rationalized by inaccessible copper cations, not reachable by dppf for a reaction. Potentially, also the space available around these cations inside the SBA-15 pores is insufficient for a Cu^{I}(dppf) complex formation. If larger dppf quantities are used for the reaction, a strong decrease of the copper-content of the samples is found by the ICP-OES measurements. This decrease is supported by ^{31}P MAS NMR spectroscopy. Thus, leaching of the copper in higher Cu^{II} : dppf stoichiometry is the reason for a lower quantity of cationic Cu^{I}(dppf) complexes observed.

Also the reaction time influences the quantified amount of Cu^{I}(dppf) complexes (see Fig. 5(c) and (d)). For a maximized amount of complexes an intermediate reaction time of 1 to 2 h is beneficial. After longer reaction times, the quantity of complexes decreases remarkably. The reason for the lower quantity of Cu^{I}(dppf) formed is not leaching, as clarified by the ICP-OES measurements and a maintained Cu-content. As discussed previously for larger dppf quantities (see Fig. 4), the initially formed complexes decompose. Summarizing, in order to maximized the amount of Cu^{I}(dppf) complexes, a Cu^{II}/dppf

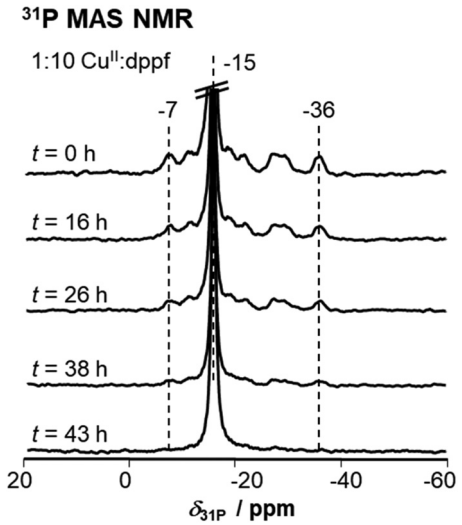

Fig. 4 ^{31}P MAS NMR after different storage time t on a Cu^{II}–[Al]SBA-15 sample after reaction with dppf in 1 : 10 stoichiometry. The intensity of the peak at −15 ppm increases over time.

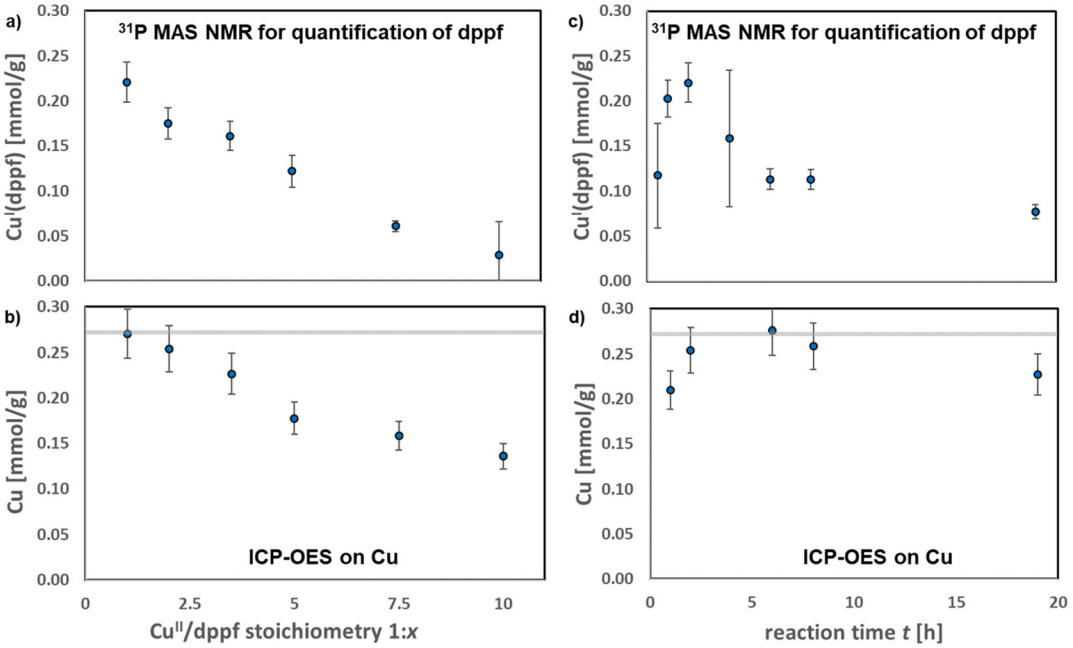

Fig. 5 Quantitative screening of Cu^{I}(dppf) complex formation conditions. In the first column a varied Cu^{II}/dppf stoichiometry after 2 h reaction time was investigated by (a) ^{31}P MAS NMR and (b) by ICP-OES on the Cu-content. On the right hand side, a reaction time screening in a 1 : 1 Cu^{II} : dppf stoichiometry was investigated by (c) ^{31}P MAS NMR and (d) by ICP-OES on the Cu-content. For the evaluation of ^{31}P MAS NMR spectra a minimum error of ±10% was assumed, even if smaller errors were obtained. Likewise, for ICP-OES measurements an error of ±10% is indicated. The initial Cu-content of the samples prior reaction is indicated by a grey bar.

stoichiometry of 1 : 1 and a reaction time of 2 h is suggested. These are the conditions that should be applied if the copper cation accessibility is investigated using dppf.

Now the accessibility of copper cations in various supports is compared using dppf. The until here applied solid, Cu–[Al] SBA-15, contains large mesopores of 6.7 nm diameter. However zeolites, frequently used heterogeneous catalysts, have micropores with a diameter far below 1 nm.[2,43] As the reaction with dppf probes the available copper cations almost quantitatively, this reaction is suited to track accessible copper cations on zeolite surfaces. In particular Cu–MCM-22 (MWW structure) is applied herein, as this material was recently shown to be active in the oxidation of methane to methanol.[13] The amount of external ion exchange sites was investigated using triphenylphosphine, which was applied on the H-form of the material according to literature.[44] In the spectrum in Fig. 6, top, a broad peak at 12 ppm indicates the formation of protonated TPP (<0.01 mmol g^{-1}). Thus, only negligible amounts of ion exchange sites are located on the external surface. The copper cations introduced by ion exchange will thus be located nearly exclusively inside the micropores or pore mouths. There, they should not be accessible for the large dppf ligand. Indeed, the ^{31}P MAS NMR spectrum (see Fig. 6, middle) after reaction with dppf shows only the peak of neat dppf at δ_{31P} = −15 ppm. No peaks of cationic Cu^{I}(dppf) complexes appear and thus no such complexes formed. It is concluded that both methods, loading with dppf and TPP probe molecules, lead to similar results. Namely, the copper

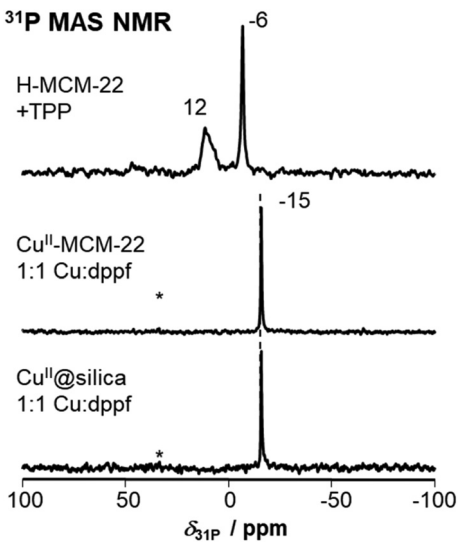

Fig. 6 ^{31}P MAS NMR spectra after TPP loading on H–MCM-22 (top) and after reaction of Cu^{II}–MCM-22 (middle) and Cu^{II}@silica (bottom) with dppf.

cations are located exclusively in MCM-22 micropores. Finally, the question arises if dppf is also reacting with Cu-particles, commonly observed side products of a copper exchange into zeolites.[46] Thus, Cu@silica synthesized by impregnation was also investigated in the reaction with dppf (see Fig. 6, bottom).

This material contains exclusively Cu-particles, as verified by the BSE detector in Fig. 1. After reaction with dppf, the ^{31}P MAS NMR spectrum contains only the slim peak of neat dppf and no peaks associated with formed complexes. Thus, the quantitative evaluation of formed Cu^{I}(dppf) complexes is a valuable tool to quantify the accessibility of copper cations. The reaction does not occur if the copper is not accessible and the formation of Cu^{I}(dppf) complexes is not observed if the copper is not in cationic position.

Conclusion

Herein a new pathway to synthesize Cu^{I}(dppf) complexes (dppf = 1,1′-bis(diphenylphosphino)ferrocene) as cations within mesoporous [Al]SBA-15 is introduced. Therefore, ion exchanged copper cations were directly reacted with dppf. These complexes can later be released from the solid by ion exchange to enable their industrial production. ^{31}P MAS NMR proves the identity of Cu^{I}(dppf) complexes after conventional ion exchange and after reaction with the solid. This is supported by ^{1}H–^{31}P FSLG HETCOR measurements. Cu^{II} cations are *in situ* reduced to Cu^{I} upon oxidation of dppf to the respective phosphine oxide. Maximized amounts of Cu^{I}(dppf) are received if a Cu^{II}/dppf stoichiometry of 1 : 1 and a reaction time of 2 h is applied during synthesis. On our Cu–[Al]SBA-15 material 81% of the initially present copper cations formed the complex. Copper leaching can occur if dppf is applied in too high stoichiometry. Also a decomposition of Cu^{I}(dppf) complexes to dppf over multiple hours is observed if unfavorable reaction conditions are applied. Cu-particles or copper located inside zeolite micropores does not contribute to the Cu^{I}(dppf) complex formation. Thus, the quantitative evaluation of peaks caused by *in situ* formed Cu^{I}(dppf) complexes is a potential tool to evaluate the amount of accessible cationic copper. The method introduced herein is thus not only of potential use for synthesizing complexes, but also for determining the accessibility of supported copper cations.

Experimental

Material preparation

The synthesis of [Al]SBA-15 by synthesis of SBA-15 and subsequent alumination was performed according to literature.[4,35] Briefly, Pluronic® P123 (16.0 g, 2.76 mmol) was dissolved in a solution of demineralized water (520 mL) and 37 wt% hydrochloric acid (80 mL) at room temperature. After addition of tetraethyl orthosilicate (36.6 mL, 165 mmol) the solution was stirred at 318 K for 7.5 h and aged at 353 K for 15.5 h under static conditions. For the synthesis of Na–[Al]SBA-15, sodium aluminate (0.12 g) was added to calcined SBA-15 (1.0 g) in water (200 mL) and the reaction mixture was stirred at room temperature for 16 h. Na–[Al]SBA-15 was obtained after calcination at 823 K for 5 h.

For the copper ion exchange, 0.45 mmol metal salt (copper(I) chloride for Cu^{I}–[Al]SBA-15 or copper(II) acetate for Cu^{II}–[Al]SBA-15) was diluted in 100 mL water, then 1 g Na–[Al]SBA-15 was added and stirred at room temperature for 24 h. After ion exchange, Cu–[Al]SBA-15 was thoroughly washed. MCM-22 was synthesized according to literature[61] and subsequently calcined at 813 K for 48 h. It was 2-fold ion exchanged with 1 M aqueous $NaNO_3$ solution and washed nitrate-free before copper ion exchange was performed, as described above. Fumed silica A200 was purchased from Evonik Industries AG, Germany. Cu@silica was obtained by wet impregnation (0.045 mmol metal salt, 10 mL demin. Water, 1 g A200) and calcined at 823 K for 5 h. The reaction with 1,1′-bis(diphenylphosphino)ferrocene (dppf) was performed by stirring a reaction mixture of Cu–[Al]SBA-15 (0.075 g) and dppf (0.3–3.0 mmol) at room temperature in ethanol or acetonitrile (50 mL) for x h (x = 0.5 to 24 h, if not otherwise stated 2 h). After measurement, the weight of the solid was determined after desorbing solvent molecules (ethanol) for 6 h at 333 K in vacuum. A complete removal of the solvent checked by ^{1}H MAS NMR spectroscopy. The reaction of dppf with Cu@silica and Cu–MCM-22 was performed analogously. Also a solid state approach for reaction between dppf and copper was applied, by mixing the respective Cu-bearing solid with neat dppf in a 1 : 2 stoichiometry (Cu : dppf) and heating it 2 h at 333 K (heating rate of 1 K min^{-1}) under N_2.

Characterization

Chemical analysis was conducted using inductively coupled plasma optical emission spectrometry (ICP-OES) on an IRIS Advantage instrument. The structure of the samples was investigated by X-ray diffraction (XRD). Therefore, a Bruker D8 diffractometer equipped with an X-ray tube for CuKα radiation (λ = 1.5418 Å) was used. The XRD patterns were recorded in a 2θ range of 0.7–5° for mesoporous and 5–55° for microporous samples. Nitrogen physisorption was performed at 77 K using a Quantachrome Autosorb 3B. Prior to measurements, the samples were activated at 623 K for 16 h. The surface of materials was evaluated using the Brunauer–Emmett–Teller (BET) equation. The micropore volume was determined according to the *V*–*t* method (deBoer) and the mesopore volume was determined as difference to the total pore volume of p/p_0 = 0.99. SEM images using SE and BSE-detectors were recorded on a Tescan Vega3 equipped with an energy dispersive X-ray spectroscopy (EDX) detector using APEX software for evaluation.

^{1}H, ^{27}Al, and ^{31}P MAS NMR spectroscopy was performed on a Bruker Avance III 400 WB spectrometer with a magnetic field of 9.4 T. The resonance frequencies were 400.1 MHz (^{1}H), 104.2 MHz (^{27}Al), and 161.9 MHz (^{31}P). ^{1}H and ^{31}P measurements were performed after π/2 excitation, whereas for qualitative ^{27}Al π/8 excitation was used. The samples for the ^{27}Al MAS NMR measurements were in a fully hydrated state. 4 mm rotor spinning rates of 8 kHz were applied, if not stated otherwise. Typical recycle delays were 5 s (qualitative ^{1}H), 20 s (quantitative ^{1}H), 5 s (^{31}P CP), and 0.5 s (^{27}Al). ^{31}P MAS NMR

direct excitation measurements were recorded using high-power proton decoupling (HPDEC) with recycle delays of 40 and 60 s, if not stated otherwise. For quantification of ^{31}P MAS NMR spectra, hydrated VPI-5 was used as an external standard, as described elsewhere.[62] ^{1}H–^{31}P FSLG HETCOR spectra were collected at 11 kHz spinning rate with a repetition time of 5 s. The indirect (^{1}H) dimension was referenced using the phenyl protons as internal standard.

For a determination of the BAS density, an ammonia loading with 60 mbar ammonia gas (Westfalen, Germany) was performed through a vacuum line. To desorb excess ammonia, a subsequent evacuation at 453 K for 2 h was performed. Activation of the samples before quantitative ^{1}H measurements was done at elevated temperature in vacuum, with a heating rate 1 K min^{-1} applying 723 K for 12 h. For quantification of ^{1}H MAS NMR spectra a dehydrated zeolite H,Na–Y (35% ammonium exchanged) was used as an external standard. The amount of external ion exchange sites was performed after activating the NH_4-form of the respective zeolites and evaluating the triphenylphosphine (TPP) loaded material by quantitative ^{31}P MAS NMR spectroscopy as described elsewhere.[44] Briefly, under N_2 the material was combined with precalculated amounts of TPP, then 0.8–1 mL of dried dichloromethane (DCM) was added, before the mixture was stirred 1 h and the vessel was finally opened under N_2 until complete evaporation of the solvent. NMR spectra were evaluated using TopSpin and Dmfit.[63]

Conflicts of interest

There is nothing to declare.

Acknowledgements

The authors want to thank Heike Fingerle for ICP-OES measurements, Faeze Tari, and Nagme Ay for N_2-physisorption measurements.

References

1 P. B. Weisz, Heterogeneous Catalysis, *Annu. Rev. Phys. Chem.*, 1970, **21**, 175–196.
2 J. Weitkamp, Zeolites and catalysis, *Solid State Ionics*, 2000, **131**, 175–188.
3 B. M. Weckhuysen and J. Yu, Recent advances in zeolite chemistry and catalysis, *Chem. Soc. Rev.*, 2015, **44**, 7022–7024.
4 V. Meynen, P. Cool and E. F. Vansant, Verified syntheses of mesoporous materials, *Microporous Mesoporous Mater.*, 2009, **125**, 170–223.
5 V. V. Butova, M. A. Soldatov, A. A. Guda, K. A. Lomachenko and C. Lamberti, Metal-organic frameworks: structure, properties, methods of synthesis and characterization, *Russ. Chem. Rev.*, 2016, **85**, 280–307.
6 M. Stöcker, Gas phase catalysis by zeolites, *Microporous Mesoporous Mater.*, 2005, **82**, 257–292.
7 M. Hunger, Br⊘nsted Acid Sites in Zeolites Characterized by Multinuclear Solid-State NMR Spectroscopy, *Catal. Rev.*, 1997, **39**, 345–393.
8 M. H. Groothaert, P. J. Smeets, B. F. Sels, P. A. Jacobs and R. A. Schoonheydt, Selective Oxidation of Methane by the Bis(μ-oxo)dicopper Core Stabilized on ZSM-5 and Mordenite Zeolites, *J. Am. Chem. Soc.*, 2005, **127**, 1394–1395.
9 K. Kvande, S. Prodinger, B. G. Solemsli, S. Bordiga, E. Borfecchia, U. Olsbye, P. Beato and S. Svelle, Cu-loaded zeolites enable the selective activation of ethane to ethylene at low temperatures and pressure, *Chem. Commun.*, 2023, **59**, 6052–6055.
10 S. Grundner, M. A. C. Markovits, G. Li, M. Tromp, E. A. Pidko, E. J. M. Hensen, A. Jentys, M. Sanchez-Sanchez and J. A. Lercher, Single-site trinuclear copper oxygen clusters in mordenite for selective conversion of methane to methanol, *Nat. Commun.*, 2015, **6**, 7546.
11 P. Vanelderen, B. E. R. Snyder, M.-L. Tsai, R. G. Hadt, J. Vancauwenbergh, O. Coussens, R. A. Schoonheydt, B. F. Sels and E. I. Solomon, Spectroscopic Definition of the Copper Active Sites in Mordenite: Selective Methane Oxidation, *J. Am. Chem. Soc.*, 2015, **137**, 6383–6392.
12 E. M. C. Alayon, M. Nachtegaal, A. Bodi and J. A. van Bokhoven, Reaction Conditions of Methane-to-Methanol Conversion Affect the Structure of Active Copper Sites, *ACS Catal.*, 2014, **4**, 16–22.
13 K. Kvande, M. Mawanga, S. Prodinger, B. G. Solemsli, J. Yang, U. Olsbye, P. Beato, E. A. Blekkan and S. Svelle, Microcalorimetry on Cu-MCM-22 Reveals Structure–Activity Relationships for the Methane-to-Methanol Reaction, *Ind. Eng. Chem. Res.*, 2023, **62**, 10939–10950.
14 M. B. Park, S. H. Ahn, A. Mansouri, M. Ranocchiari and J. A. van Bokhoven, Comparative Study of Diverse Copper Zeolites for the Conversion of Methane into Methanol, *ChemCatChem*, 2017, **9**, 3705–3713.
15 C. Copéret, A. Comas-Vives, M. P. Conley, D. P. Estes, A. Fedorov, V. Mougel, H. Nagae, F. Núñez-Zarur and P. A. Zhizhko, Surface Organometallic and Coordination Chemistry toward Single-Site Heterogeneous Catalysts: Strategies, Methods, Structures, and Activities, *Chem. Rev.*, 2016, **116**, 323–421.
16 M. K. Samantaray, S. K. Mishra, A. Saidi and J.-M. Basset, Surface organometallic chemistry: A sustainable approach in modern catalysis, *J. Organomet. Chem.*, 2021, **945**, 121864.
17 R. Augustine, S. Tanielyan, S. Anderson and H. Yang, A new technique for anchoring homogeneous catalysts, *Chem. Commun.*, 1999, 1257–1258, DOI: 10.1039/A903205C.
18 D. T. Genna, A. G. Wong-Foy, A. J. Matzger and M. S. Sanford, Heterogenization of Homogeneous Catalysts in Metal–Organic Frameworks via Cation Exchange, *J. Am. Chem. Soc.*, 2013, **135**, 10586–10589.
19 M. K. Samantaray, E. Pump, A. Bendjeriou-Sedjerari, V. D'Elia, J. D. A. Pelletier, M. Guidotti, R. Psaro and

J.-M. Basset, Surface organometallic chemistry in heterogeneous catalysis, *Chem. Soc. Rev.*, 2018, **47**, 8403–8437.

20 C. Copéret, Single-Sites and Nanoparticles at Tailored Interfaces Prepared via Surface Organometallic Chemistry from Thermolytic Molecular Precursors, *Acc. Chem. Res.*, 2019, **52**, 1697–1708.

21 S. R. Docherty and C. Copéret, Deciphering Metal–Oxide and Metal–Metal Interplay via Surface Organometallic Chemistry: A Case Study with CO2 Hydrogenation to Methanol, *J. Am. Chem. Soc.*, 2021, **143**, 6767–6780.

22 C. Copéret, F. Allouche, K. W. Chan, M. P. Conley, M. F. Delley, A. Fedorov, I. B. Moroz, V. Mougel, M. Pucino, K. Searles, K. Yamamoto and P. A. Zhizhko, Bridging the Gap between Industrial and Well-Defined Supported Catalysts, *Angew. Chem., Int. Ed.*, 2018, **57**, 6398–6440.

23 S. E. Maier, O. Bunjaku, E. Kaya, M. Dyballa, W. Frey and D. P. Estes, Surface immobilized Cu-1,10-phenanthroline complexes with α-aminophosphonate groups in the 5-position as heterogenous catalysts for efficient atom-transfer radical cyclizations, *Dalton Trans.*, 2023, **52**, 8442–8448.

24 C. Rieg, M. Kirchhof, K. Gugeler, A.-K. Beurer, L. Stein, K. Dirnberger, W. Frey, J. R. Bruckner, Y. Traa, J. Kästner, S. Ludwigs, S. Laschat and M. Dyballa, Determination of accessibility and spatial distribution of chiral Rh diene complexes immobilized on SBA-15 via phosphine-based solid-state NMR probe molecules, *Catal. Sci. Technol.*, 2023, **13**, 410–425.

25 S. R. Kousik, F. Ziegler, D. Sipp, A. Rodríguez-Camargo, H. Solodenko, W. Gassner, G. Schmitz, B. V. Lotsch, M. R. Buchmeiser, K. Koynov and P. Atanasova, Imaging the Permeability and Passivation Susceptibility of SiO_2 Nanosphere-Based Mesoporous Supports for Molecular Heterogeneous Catalysis under Confinement, *ACS Appl. Nano Mater.*, 2022, **5**, 14733–14745.

26 M. Schnierle, S. Klostermann, E. Kaya, Z. Li, D. Dittmann, C. Rieg, D. P. Estes, J. Kästner, M. R. Ringenberg and M. Dyballa, How Solid Surfaces Control Stability and Interactions of Supported Cationic CuI(dppf) Complexes—A Solid-State NMR Study, *Inorg. Chem.*, 2023, **62**, 7283–7295.

27 D. Schweinfurth, N. Büttner, S. Hohloch, N. Deibel, J. Klein and B. Sarkar, Heterobimetallic Cu–dppf (dppf = 1,1′-Bis (diphenylphosphino)ferrocene) Complexes with "Click" Derived Ligands: A Combined Structural, Electrochemical, Spectroelectrochemical, and Theoretical Study, *Organometallics*, 2013, **32**, 5834–5842.

28 C. Bravo, M. P. Robalo, F. Marques, A. R. Fernandes, D. A. Sequeira, M. F. M. Piedade, M. H. Garcia, M. J. V. de Brito and T. S. Morais, First heterobimetallic Cu(i)–dppf complexes designed for anticancer applications: synthesis, structural characterization and cytotoxicity, *New J. Chem.*, 2019, **43**, 12308–12317.

29 L. Bemi, H. C. Clark, J. A. Davies, C. A. Fyfe and R. E. Wasylishen, Studies of phosphorus(III) ligands and their complexes of nickel(II), palladium(II), and platinum (II) immobilized on insoluble supports by high-resolution solid-state phosphorus-31 NMR using magic-angle spinning techniques, *J. Am. Chem. Soc.*, 1982, **104**, 438–445.

30 G. A. Bowmaker, J. V. Hanna, R. D. Hart, P. C. Healy, S. P. King, F. Marchetti, C. Pettinari, B. W. Skelton, A. Tabacaru and A. H. White, Mechanochemical and solution synthesis, X-ray structure and IR and 31P solid state NMR spectroscopic studies of copper(i) thiocyanate adducts with bulky monodentate tertiary phosphine ligands, *Dalton Trans.*, 2012, **41**, 7513–7525.

31 G. A. Bowmaker, J. V. Hanna, S. P. King, F. Marchetti, C. Pettinari, A. Pizzabiocca, B. W. Skelton, A. N. Sobolev, A. Tăbăcaru and A. H. White, Complexes of Copper(I) Thiocyanate with Monodentate Phosphine and Pyridine Ligands and the P(,N)-Donor Diphenyl(2-pyridyl)phosphine, *Eur. J. Inorg. Chem.*, 2014, **2014**, 6104–6116.

32 M. Dyballa, Solid-State NMR Probe Molecules for Catalysts and Adsorbents: Concepts, Quantification, Accessibility, and Spatial Distribution, *Energy Fuels*, 2023, **37**, 18517–18559.

33 D. S. Zasukhin, I. A. Kasyanov, Y. G. Kolyagin, A. I. Bulygina, K. C. Kharas and I. I. Ivanova, Evaluation of Zeolite Acidity by 31P MAS NMR Spectroscopy of Adsorbed Phosphine Oxides: Quantitative or Not?, *ACS Omega*, 2022, **7**, 12318–12328.

34 A. Zheng, S.-B. Liu and F. Deng, 31P NMR Chemical Shifts of Phosphorus Probes as Reliable and Practical Acidity Scales for Solid and Liquid Catalysts, *Chem. Rev.*, 2017, **117**, 12475–12531.

35 Z. Li, M. Benz, C. Rieg, D. Dittmann, A.-K. Beurer, D. Häussermann, B. Arstad and M. Dyballa, The alumination mechanism of porous silica materials and properties of derived ion exchangers and acid catalysts, *Mater. Chem. Front.*, 2021, **5**, 4254–4271.

36 V. L. Sushkevich, R. Verel and J. A. van Bokhoven, Pathways of Methane Transformation over Copper-Exchanged Mordenite as Revealed by In Situ NMR and IR Spectroscopy, *Angew. Chem., Int. Ed.*, 2020, **59**, 910–918.

37 N. F. Dummer, D. J. Willock, Q. He, M. J. Howard, R. J. Lewis, G. Qi, S. H. Taylor, J. Xu, D. Bethell, C. J. Kiely and G. J. Hutchings, Methane Oxidation to Methanol, *Chem. Rev.*, 2023, **123**, 6359–6411.

38 M. Dyballa, K. Thorshaug, D. K. Pappas, E. Borfecchia, K. Kvande, S. Bordiga, G. Berlier, A. Lazzarini, U. Olsbye, P. Beato, S. Svelle and B. Arstad, Zeolite Surface Methoxy Groups as Key Intermediates in the Stepwise Conversion of Methane to Methanol, *ChemCatChem*, 2019, **11**, 5022–5026.

39 K. A. Lomachenko, E. Borfecchia, C. Negri, G. Berlier, C. Lamberti, P. Beato, H. Falsig and S. Bordiga, The Cu-CHA deNOx Catalyst in Action: Temperature-Dependent NH3-Assisted Selective Catalytic Reduction Monitored by Operando XAS and XES, *J. Am. Chem. Soc.*, 2016, **138**, 12025–12028.

40 A. A. Kolganov, A. A. Gabrienko, S. A. Yashnik, E. A. Pidko and A. G. Stepanov, Nature of the Surface Intermediates Formed from Methane on Cu-ZSM-5 Zeolite: A Combined Solid-State Nuclear Magnetic Resonance and Density

Functional Theory Study, *J. Phys. Chem. C*, 2020, **124**, 6242–6252.

41 C. Rieg, D. Dittmann, Z. Li, A. Kurtz, I. Lorenz, D. P. Estes, M. Buchmeiser, M. Dyballa and M. Hunger, Noble metal location in porous supports determined by reaction with phosphines, *Microporous Mesoporous Mater.*, 2021, **310**, 110594.

42 C. Rieg, D. Dittmann, Z. Li, R. Lawitzki, K. Gugeler, S. Maier, G. Schmitz, J. Kastner, D. P. Estes and M. Dyballa, Quantitative Distinction between Noble Metals Located in Mesopores from Those on the External Surface, *Chem. – Eur. J.*, 2021, **27**, 17012–17023.

43 C. Baerlocher and L. B. McCusker, Database of Zeolite Structures: **https://www.iza-structure.org/databases/**, (accessed 08.09., 2023).

44 C. Rieg, Z. Li, A. Kurtz, M. Schmidt, D. Dittmann, M. Benz and M. Dyballa, A Method for the Selective Quantification of Brønsted Acid Sites on External Surfaces and in Mesopores of Hierarchical Zeolites, *J. Phys. Chem. C*, 2021, **125**, 515–525.

45 Z. Li, D. Dittmann, C. Rieg, M. Benz and M. Dyballa, Confinement and surface sites control methanol adsorbate stability on MFI zeolites, SBA-15, and a silica-supported heteropoly acid, *Catal. Sci. Technol.*, 2022, **12**, 2265–2277.

46 M. Dyballa, D. K. Pappas, E. Borfecchia, P. Beato, U. Olsbye, K. P. Lillerud, B. Arstad and S. Svelle, Tuning the material and catalytic properties of SUZ-4 zeolites for the conversion of methanol or methane, *Microporous Mesoporous Mater.*, 2018, **265**, 112–122.

47 M. Hunger, Multinuclear solid-state NMR studies of acidic and non-acidic hydroxyl protons in zeolites, *Solid State Nucl. Magn. Reson.*, 1996, **6**, 1–29.

48 Y. Jiang, J. Huang, W. Dai and M. Hunger, Solid-state nuclear magnetic resonance investigations of the nature, property, and activity of acid sites on solid catalysts, *Solid State Nucl. Magn. Reson.*, 2011, **39**, 116–141.

49 W. Yang, Z. Wang, J. Huang and Y. Jiang, Qualitative and Quantitative Analysis of Acid Properties for Solid Acids by Solid-State Nuclear Magnetic Resonance Spectroscopy, *J. Phys. Chem. C*, 2021, **125**, 10179–10197.

50 D. Coster, A. L. Blumenfeld and J. J. Fripiat, Lewis Acid Sites and Surface Aluminum in Aluminas and Zeolites: A High-Resolution NMR Study, *J. Phys. Chem.*, 1994, **98**, 6201–6211.

51 H. Yu, X. Tan, G. M. Bernard, V. V. Terskikh, J. Chen and R. E. Wasylishen, Solid-State 63Cu, 65Cu, and 31P NMR Spectroscopy of Photoluminescent Copper(I) Triazole Phosphine Complexes, *J. Phys. Chem. A*, 2015, **119**, 8279–8293.

52 E. Borfecchia, D. K. Pappas, M. Dyballa, K. A. Lomachenko, C. Negri, M. Signorile and G. Berlier, Evolution of active sites during selective oxidation of methane to methanol over Cu-CHA and Cu-MOR zeolites as monitored by operando XAS, *Catal. Today*, 2019, **333**, 17–27.

53 L. Peng, P. J. Chupas and C. P. Grey, Measuring Brønsted Acid Densites in Zeolite HY with Diphosphine Molecules and Solid State NMR Spectroscopy, *J. Am. Chem. Soc.*, 2004, **126**, 12254–12255.

54 L. Peng and C. P. Grey, Diphosphine probe molecules and solid-state NMR investigations of proximity between acidic sites in zeolite HY, *Microporous Mesoporous Mater.*, 2008, **116**, 277–283.

55 D. J. Zalewski, P. J. Chu, P. N. Tutunjian and J. H. Lunsford, The oxidation of trimethylphosphine in zeolite Y: a solid-state NMR study, *Langmuir*, 1989, **5**, 1026–1030.

56 C. Rieg, D. Dittmann, Z. Li, A. Kurtz, E. Kaya, S. Peters, B. Kunkel, M. Parlinska-Wojtan, S. Wohlrab, A. M. Abdel-Mageed and M. Dyballa, Introducing a Novel Method for Probing Accessibility, Local Environment, and Spatial Distribution of Oxidative Sites on Solid Catalysts Using Trimethylphosphine, *J. Phys. Chem. C*, 2022, **126**, 13213–13223.

57 B. Hu and I. D. Gay, Probing Surface Acidity by 31P Nuclear Magnetic Resonance Spectroscopy of Arylphosphines, *Langmuir*, 1999, **15**, 477–481.

58 B. Hu and I. D. Gay, Acid Sites on SiO_2–Al_2O_3 Monolayer Catalysts: 31P NMR Probes of Strength and Accessibility, *J. Phys. Chem. B*, 2001, **105**, 217–219.

59 C. Bornes, D. Stosic, C. F. G. C. Geraldes, S. Mintova, J. Rocha and L. Mafra, Elucidating the Nature of the External Acid Sites of ZSM-5 Zeolites Using NMR Probe Molecules, *Chem. – Eur. J.*, 2022, **28**, e202201795.

60 G. A. Bowmaker, S. E. Boyd, J. V. Hanna, R. D. Hart, P. C. Healy, B. W. Skelton and A. H. White, Structural and spectroscopic studies on three-coordinate complexes of copper(i) halides with tricyclohexylphosphine, *J. Chem. Soc., Dalton Trans.*, 2002, 2722–2730, DOI: **10.1039/B111121N**.

61 S. Unverricht, M. Hunger, S. Ernst, H. G. Karge and J. Weitkamp, in *Studies in Surface Science and Catalysis*, ed. J. Weitkamp, H. G. Karge, H. Pfeifer and W. Hölderich, Elsevier, 1994, vol. 84, pp. 37–44.

62 M. Dyballa, C. Rieg, D. Dittmann, Z. Li, M. Buchmeiser, B. Plietker and M. Hunger, Potential of triphenylphosphine as solid-state NMR probe for studying the noble metal distribution on porous supports, *Microporous Mesoporous Mater.*, 2020, **293**, 109778.

63 D. Massiot, F. Fayon, M. Capron, I. King, S. Le Calvé, B. Alonso, J.-O. Durand, B. Bujoli, Z. Gan and G. Hoatson, Modelling one- and two-dimensional solid-state NMR spectra, *Magn. Reson. Chem.*, 2002, **40**, 70–76.